# Cold hydrogen blowdown release: an inter-comparison study

**S.G. Giannissi[1,*], A.G. Venetsanos[1], D. Cirrone[2], V. Molkov[2], Z. Ren[3], J. Wen[3], A. Friedrich[4], A. Veser[4]**

**[1] Environmental Research Laboratory, National Center for Scientific Research Demokritos, Aghia Paraskevi, Athens, 15341, Greece, sgiannissi@ipta.demokritos.gr**

**[2] HySAFER Centre, University of Ulster, Newtownabbey BT37 0QB, UK**

**[3] School of Engineering, University of Warwick, Coventry, CV4 7AL, United Kingdom**

**[4] Pro-Science GmbH, Parkstrasse 9, Ettlingen, 76275, Germany**

**ABSTRACT**

Hydrogen dispersion in stagnant environment resulting from blowdown of a vessel storing the gas at cryogenic temperature is simulated using different CFD codes and modelling strategies. The simulations are based on the DISCHA experiments that were carried out by Karlsruhe Institute of Technology (KIT) and Pro-Science (PS). The selected test for the current study involves hydrogen release from a 2.815 $dm^3$ volume tank with an initial pressure of 200 barg and temperature 80 K. During the release, the hydrogen pressure in the tank gradually decreased. A total of about 139 gr hydrogen is released through a 4 mm diameter. The temperature time series and the temperature decay rate of the minimum value predicted by the different codes are compared with each other and with the experimentally measured ones. Recommendations for future experimental setup and for modeling approaches for similar releases are provided based on the present analysis. The work is carried out within the EU-funded project, PRESLHY.

Keywords: hydrogen blowdown, CFD, cryogenic, small-scale

## 1.0 INTRODUCTION

In the last years, hydrogen technology is introduced more and more in transport sector. The more effective option for this kind of applications is liquid hydrogen (LH2) due to its high energy density. This generates the need of pre-normative research for the safer use of LH2. PRESLHY is an EU-funded project that seeks to close certain knowledge gaps related to LH2 safety and to provide safety recommendations. In this framework several experiments with cryogenic hydrogen release and dispersion have been performed within PRELHY and its behavior is studied. In parallel, Computational Fluid Dynamics (CFD) codes are used to simulate these experiments, in order to assist the understanding of the underlying phenomena and to be validated against well-defined experiments.

This work deals with the CFD modeling of hydrogen dispersion resulting from blowdown cryogenic release. CFD modeling of such flows can be challenging and any model/approach should be first validated against experiments, in order to enable its future use for the production of reliable safety assessments. The experiments [1] performed by Karlsruhe Institute of Technology (KIT) and Pro-Science (PS) were used for the validation. They involve hydrogen release from a 200 barg vessel at 80 K through a 4 mm nozzle.

In this CFD study three project partners participated with different CFD codes and modeling strategies and the computational results are evaluated against the experiments. The softwares that were used is: ADREA-HF, ANSYS Fluent and OpenFOAM. More details about the modeling strategy that each partner followed can be found in Section 3.0.

To simulate the high-pressure release all partners used the concept of notional nozzle approach. Based on this approach simple calculations are performed in the high-compressible region between the nozzle and the location where the jet is fully expanded to ambient pressure. Since 1984 when the notional nozzle concept was first introduced by Birch [2] several other approaches have been developed with different assumptions. A review and evaluation of some of the available notional approaches is presented in [3]. In [4], the CFD model was also used to simulate the high-compressible region of the under-expanded jet and compared against experiment and several notional approaches. It was shown that the notional nozzle approaches gave good predictions, while CFD underestimated the concentration. This underestimation of CFD model can be attributed to the higher diffusion due to

small turbulent Schmidt number or large air entrainment. More research should be carried out to study the CFD modeling of under-expanded hydrogen jet.

The comparison of the CFD results with the measurements showed fairly good agreement among predictions and simulations. The CFD results and the temperature measurements indicated also that the experimental configuration for concentration measurements led to inaccuracies regarding the arrival time of the mixture. The entire analysis is presented and discussed in Section Results and discussion.

## 2.0 DISCHA EXPERIMENTAL DESCRIPTION

More than 200 hydrogen blow-down experiments were conducted with the DisCha-facility at Karlsruhe Institute of Technology and in collaboration with Pro-Science [1]. Half of the experiments were performed at cryogenic temperatures (approx. 80 K). The DisCha-facility is consisted of a 2.815 $dm^3$ internal volume vessel, which is fastened in an insulated box for the LN2 pool cooling. The discharge line and associated dimensions are shown in Figure 1, left.

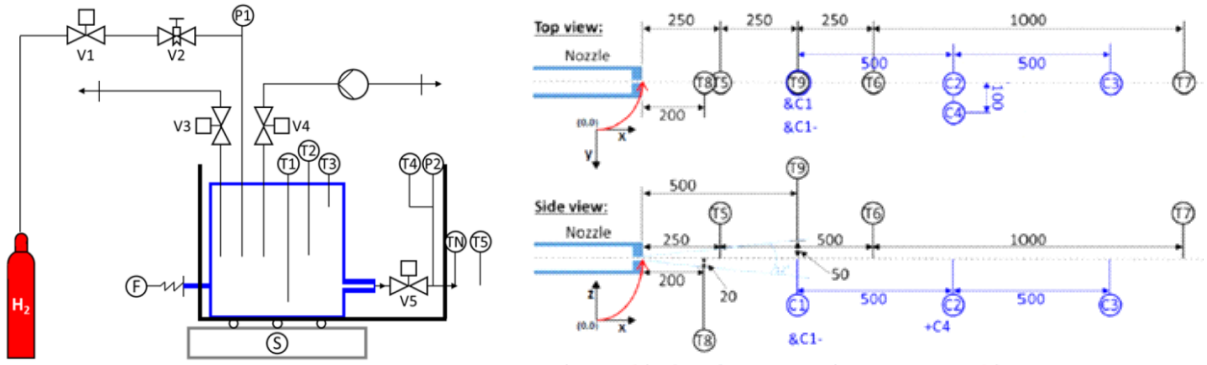


Figure 1. Sketch of the DISCHA facility (left) and the H2-sensors and thermocouples position (right).

Pressure was measured inside the tank (P1) and after the valve (P2). Temperatures were measured inside the vessel (T1, T2, T3), after the valve (T4) and at the nozzle (TN). T4 is welded into the line to measure the temperature inside it. TN is mounted from the outside in a hole in the material of the stainless steel nozzle aperture with no direct contact to the flowing gas. Thus, T4 measurements are considered a closer indication of the nozzle temperature.

For the current CFD study the trial 20190528_104204 was chosen. This trial involves blowdown release of hydrogen at 200 barg and 80 K through a 4 mm nozzle. At the nozzle the conditions were such that only vapor hydrogen was released.

Five thermocouples and five H2-sensors were placed at several points to monitor the mixture distribution (see Figure 1, right). Three thermocouples, T5, T6 and T7, were placed along the release centreline (x-axis) at 0.25, 0.75 and 1.75 m distance from the nozzle, respectively, while T8 was placed 0.02 m below the jet centreline along z-axis at 0.2 m distance from the nozzle. T9 was placed 0.05 above the jet centreline along z-axis at 0.5 m distance from the nozzle. Three H2-sensors, C1, C2 and C3 were placed along the release centreline at 0.5, 1 and 1.5 m, respectively, while one sensor was placed at 1 m from the nozzle and 0.1 m offset along the y-axis (lateral direction). The fifth sensor (C1-) had different configuration and was used for comparison, thus it placed in the same location as C1.

The H2-sensors were quite large, thus in order not to disturb the flow they were not mounted physically to the positions shown in Figure 1, right. They were connected to these positions via thin plastic tubes of 2.55 m length. One small pump was used to supply all sensors with the same volume flow of test atmosphere during the measurements. Due to this configuration there is a delay time in concentration records. PS performed pre-experiments to determine this delay time. They exposed the open tip of the plastic tube with pure or diluted hydrogen (20% H2, forming gas) from a balloon (without forcing an additional flow of the test gas in the tube). A similar delay time of 2 s was found

for all sensors from the opening of the hydrogen balloon to the first increase in the signals of the hydrogen sensors. However, in the actual experiments which have widely different conditions this delay seems to be a) underestimated and b) different for each sensor location, i.e. depending on the flow conditions. This also means that an error might be introduced in the concentration gradients during the blowdown release.

The thermocouple measurements showed that the minimum values were achieved almost at time zero at all positons. Taking into account the correlation between temperature and concentration we consider the thermocouple arrival times as indicative for the concentration arrival time as well.

Finally, there was a delay from the time that experiment was triggered until the time that the valve starts to open and the pressure just upstream the nozzle, P4, starts to increase. The time that P4 starts to increase is considered time zero for the experiments and the time series were synchronized accordingly. This response time was 0.065 sec for this test. Additional delay until the valve is fully open has not been estimated and was not taken into account in time synchronization.

## 3.0 CFD SIMULATIONS

### 3.1 NCSRD modeling strategy

To model hydrogen dispersion the CFD code ADREA-HF has been used. The 3D time dependent conservation equations are solved. Mass, momentum, static enthalpy conservation equation for the mixture and the hydrogen mass fraction conservation equation are solved based on the following equations:

$$\frac{\partial \rho}{\partial t} + \frac{\partial \rho u_i}{\partial x_i} = 0 \tag{1}$$

$$\frac{\partial \rho u_i}{\partial t} + \frac{\partial \rho u_i u_j}{\partial x_j} = -\frac{\partial P}{\partial x_i} + \frac{\partial}{\partial x_j}\left( (\mu + \mu_t)\left( \frac{\partial u_i}{\partial x_j} + \frac{\partial u_j}{\partial x_i} \right) \right) + \rho g_i \tag{2}$$

$$\begin{aligned} \frac{\partial \rho h}{\partial t} + \frac{\partial \rho u_i h}{\partial x_i} = \frac{dP}{dt} + \frac{\partial}{\partial x_i}\left( (\lambda + \lambda_t)\frac{\partial T}{\partial x_i} \right) \\ + \frac{\partial}{\partial x_i}\left( \rho \sum_{k \neq a} D_{q_k} \left( h_{v_k} - h_{v_a} \right) \frac{\partial q_{v_k}}{\partial x_i} \right) + \frac{\partial}{\partial x_i}\left( \sum_k \frac{\mu_t}{Sc_t} h_k \frac{\partial q_k}{\partial x_i} \right) \end{aligned} \tag{3}$$

$$\frac{\partial \rho q_p}{\partial t} + \frac{\partial \rho u_j q_p}{\partial x_j} = \frac{\partial}{\partial x_j}\left( \left( \rho D_p + \frac{\mu_t}{Sc_t} \right) \frac{\partial q_p}{\partial x_j} \right) \tag{4}$$

where $\rho$ - mixture density, kg/m$^3$; $u$ - velocity, m/s; P - pressure, Pa; $g$ - gravitational acceleration, m/s$^2$; T - temperature, K; $\mu, \mu_t$ - laminar and turbulent viscosity respectively, kg/m/s; $\lambda, \lambda_t$ - laminar and turbulent thermal conductivity respectively, W/m/K; $Sc_t$ - turbulent Schmidt number, dimensionless; D - molecular diffusivity, m$^2$/s; h - enthalpy, J/kg; q - total mass fraction (vapor and liquid if it exists). The turbulent Schmidt is set equal to 0.72. The subscripts i and j denote the Cartesian x, y and z coordinates, index p denotes the component p, index v is for the vapor phase and index a is for air.

For the turbulence modeling the standard k-epsilon with extra buoyance terms [5] is employed.

#### 3.1.1 Release modelling

A challenging task for the simulation of this experiment was the release blowdown modeling. Inside the tank there is high-pressure cryogenic hydrogen, which is released through a discharge line with several components (e.g. valve and nozzle). As shown in Figure 1 a small part of the discharge line

and the nozzle are outside the LN2 cooling box and thus additional heat transfer from the environment might occur. To accurately model the blowdown release steady state isentropic process is performed from the measured tank conditions to the nozzle conditions taking into account the pressure losses along the discharge line and all its elements using the discharge tool presented in [6]. Figure 2 shows the experimental mass flow rate with respect to the calculated mass flow rate and the calculated nozzle pressure and temperature.

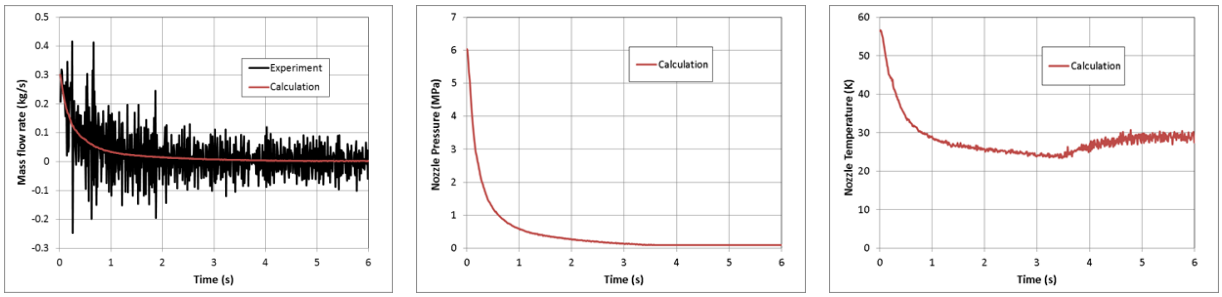


Figure 2. The experimental versus the calculated mass flow rate and the calculated nozzle pressure and temperature.

As shown in Figure 2, the pressure at the nozzle is higher than ambient pressure until around 3.4 s. This means that an under-expanded jet is formed downwind the nozzle. To model the fully compressible region of the under-expanded jet the notional nozzle concept was used. Based on the notional nozzle approach the real nozzle is replaced by a fictitious nozzle where the jet is fully expanded and the pressure is equal to ambient. To estimate the rest conditions in the fictitious area several approaches have been developed over the last decades. In some approaches the notional velocity is assumed equal to sonic, while in other approaches supersonic velocity is imposed by solving the momentum balance from the real nozzle to the notional nozzle. In these approaches higher momentum is introduced in the computational domain. On the other hand, in the approaches with sonic velocities larger notional diameter is calculated to conserve the mass flow rate. The temperature at the notional nozzle can either be assumed equal to a specific value, e.g. equal to the nozzle temperature (or equal to ambient in room temperature releases) or enthalpy conservation equation can be solved to predict it. In the second approach lower that the nozzle temperature is predicted, this in turn might lead to two-phase conditions at notional nozzle.

NCSRD used the approach that solves 1D conservation mass and momentum equations [7] from the nozzle to the notional nozzle and assumes that the temperature is equal to the nozzle temperature. Based on this approach supersonic velocity is predicted at the notional nozzle. For the calculations the NCSRD discharge tool was used, which applies the NIST EoS that is based on explicit modeling of the Helmholtz free energy.

Figure 3 shows the temperature, velocity and diameter that NCSRD used at notional nozzle. The notional nozzle conditions were somehow smoothed to avoid convergence problems in the CFD dispersion problem. UU and UWAR respective values are also shown for comparison.

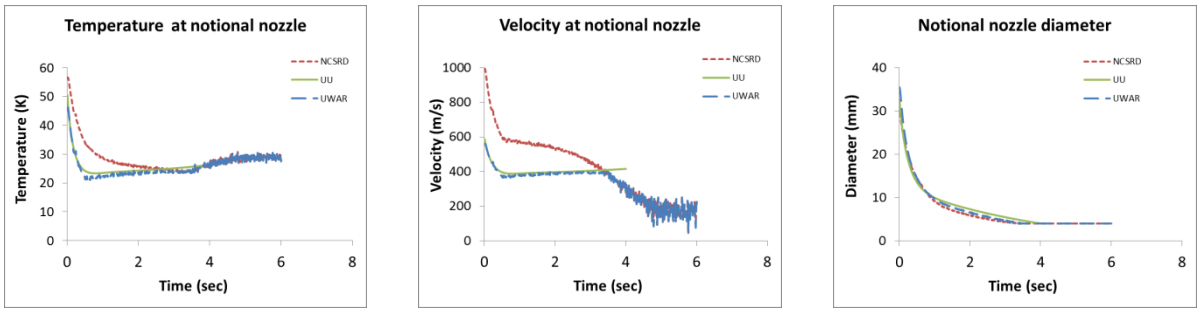


Figure 3. The transient conditions at notional nozzle that were used in NCSRD, UU and UWAR simulations.

Transient source terms (with given velocity, temperature and notional nozzle area time histories) are introduced in two cells at the release location to model the transient jet.

### 3.1.2 Computational grid and numerical details

The computational domain is extended in the x-axis 100 mm upwind the source and 12 m downwind and in the y-axis is extended 2 m. Symmetry along the y-axis is assumed. In the z-axis the domain is extended 2 m above the source and 1.1 m below. A Cartesian grid with 306 680 cells in total is designed. Two cells were used to discretize the symmetric source area. Each cell was equal to the ¼ of the initial notional nozzle. Very small expansion ratio (1.05 and 1.08) is used in the close vicinity of the source in all directions and further downwind the ratio is increased until the maximum of 1.12.

Constant pressure boundary condition is imposed in all boundaries except the bottom where wall boundaries are set and except for the symmetry plane.

Higher order numerical scheme (MUSCL) was used for the discretization of convective terms, central differences for the diffusive terms and 1st order upwind for time integration. Under-relaxation factor equal to 0.7 was used in all variables. The time step was variant and very small ($10^{-4}$ order of magnitude at the initial stage of the blowdown to $10^{-3}$ at the later stage when mass flow rate decreased).

## 3.2 UU modeling strategy

ANSYS Fluent V20.2 was used as a platform for CFD computations. An approach solving the Reynolds-averaged Navier-Stokes (RANS) conservations for mass, momentum, energy and species was selected:

$$\frac{\partial \rho}{\partial t} + \frac{\partial (\rho u_i)}{\partial x_i} = 0, \tag{5}$$

$$\frac{\partial (\rho u_i)}{\partial t} + \frac{\partial (\rho u_i u_j)}{\partial x_i} = -\frac{\partial \rho}{\partial x_i} + \frac{\partial}{\partial x_i}(\mu + \mu_t)\left(\frac{\partial u_i}{\partial x_j} + \frac{\partial u_j}{\partial x_i} - \frac{2}{3}\frac{\partial u_k}{\partial x_k}\delta_{ij}\right) + \rho g_i, \tag{6}$$

$$\frac{\partial (\rho E)}{\partial t} + \frac{\partial}{\partial x_i}\left(u_i(\rho E + p)\right) \tag{7}$$

$$= \frac{\partial}{\partial x_i}\left[\left(k + \frac{\mu_t c_p}{Pr_t}\right)\frac{\partial T}{\partial x_i} - \sum_m h_m\left(-\left(\rho D_m + \frac{\mu_t}{Sc_t}\right)\frac{\partial Y_m}{\partial x_i}\right) + u_i(\mu + \mu_t)\left(\frac{\partial u_i}{\partial x_j} + \frac{\partial u_j}{\partial x_i} - \frac{2}{3}\frac{\partial u_k}{\partial x_k}\delta_{ij}\right)\right] + S_E,$$

$$\frac{\partial \rho Y_m}{\partial t} + \frac{\partial}{\partial x_i}(\rho u_i Y_m) = \frac{\partial}{\partial x_i}\left[\left(\rho D_m + \frac{\mu_t}{Sc_t}\right)\frac{\partial Y_m}{\partial x_i}\right] + S_m. \tag{8}$$

where $\rho$ is the density, t is the time, i,j and k corresponds to the Cartesian coordinates and $u$ the velocity components, $p$ is the pressure, $\mu_t$ is the turbulent dynamic viscosity, $\delta_{ij}$ is the Kronecker symbol, $g_i$ is the gravity acceleration, $E$ is the total energy, $c_p$ is the specific heat at constant pressure, $Pr_t$ and $Sc_t$ are the turbulent Prandtl and Schmidt numbers equal to 0.85 and 0.70 respectively, $D_m$ is the molecular diffusivity of the species $m$, $Y_m$ is the corresponding mass fraction, $S_E$ and $S_m$ are the source terms for energy and chemical specie.

Turbulence was accounted using the standard k-ε turbulence model (Launder and Spalding, 1972) with buoyancy terms.

### 3.2.1 Release modelling

The release from the high-pressure hydrogen storage (200 bar) results in an under-expanded jet. The storage pressure and temperature dynamics during the tank blowdown were modelled by using a non-adiabatic model based on methodology by [8]. The model takes into account convective heat transfer at the internal and external walls. Nusselt correlations are employed to calculate the convective heat transfer coefficients. Conduction through the wall is calculated by solving an unsteady heat transfer

one-dimensional equation though the finite difference method. In this formulation, the non-ideal behaviour of cryogenic hydrogen is taken into account by using NIST EOS, instead of Abel-Noble as in [8], by implementing CoolProp database to evaluate hydrogen thermodynamic parameters [9]. The hydrogen flow parameters at the real and notional nozzle were modelled by using the under-expanded jet theory in [10], which is based on mass and energy conservation equations. The approach was modified to employ NIST EOS as presented in [11]. The flow is characterized by uniform sonic velocity and ambient pressure at the notional nozzle, simplifying significantly the problem by considering the jet flow at the notional nozzle as completely expanded. A discharge coefficient of 0.7 is applied to take into account losses in the release system. Figure 4 shows the comparison between the resulting pressure and temperature dynamics in the storage and the calculated mass flow rate with experimental measurements.

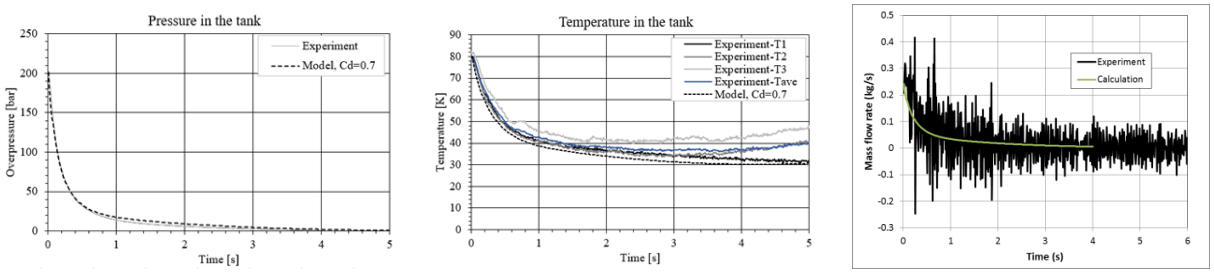


Figure 4. Pressure and temperature dynamics in the storage during blowdown and comparison of calculated mass flow rate with experiment.

Employing the notional nozzle diameter as inflow boundary with specified flow velocity would require a change of the numerical grid because the release conditions in the notional nozzle and its diameter are changing during blowdown process. To avoid the change of grid, the release of hydrogen was reproduced through the volumetric source implementation of the notional nozzle approach during the tank blowdown [10]. This approach is based on the evaluation of transient source terms for mass, momentum, energy, turbulent kinetic energy and turbulent dissipation rate depending which vary in time to reflect on the changing dynamics of properties at the notional nozzle. Source terms are applied to a constant cubic volume, thus responsible for the hydrogen release. The cube length is 3.3 cm and it corresponds to the value of the notional nozzle at the beginning of the tank blowdown.

### 3.2.2 Computational grid and numerical details

The calculation domain is rectangular with dimensions 8x3x4 m. All boundaries are modelled as no-slip walls with exception of the side perpendicular to the release axis, which is considered as a pressure-outlet with gauge pressure equal to 0 Pa. The numerical grid is hexahedral. The volumetric releases source is located at 0.5 m from the back wall and 1.11 m height from the ground. The volumetric source exit is discretized by 2x2 cells, which have a minimum size of 1.7 cm. The cell size dimensions are increased with a growth ratio equal to 1.1. The total number of control volumes is 308 892. The ambient temperature is 288 K, the ambient pressure is 1 bar and normal air composition is considered. Pressure-based solver was employed along with the compressible gas assumption. SIMPLE procedure is chosen for velocity-pressure coupling, whereas convective terms are discretized using the second order upwind. A constant time step equal to $1 \cdot 10^{-2}$ s is applied. Time step sensitivity analysis was performed by decreasing the time step to 0.005 s. Temperature dynamics at two locations 2 cm away from T5 and T6 was used for comparison and was seen to not show significant differences for a time larger than 0.05s.

## 3.3 UWAR modeling strategy

Large eddy simulation (LES) of the unsteady cryogenic hydrogen jet during the blowdown process is conducted using rhoReactingFOAM, which is a density-based multi-species compressible flow solver within the frame of open-source CFD code OpenFOAM. In LES all variables are decomposed into resolved and unresolved (sub-grid) components by filtering Navier–Stokes equations. The governing equations are solved for three conservative variables, specifically density, momentum density, and total energy density. A transport equation is also applied in order to consider the mixing of multiple species. One-equation eddy-viscosity SGS model for compressible flows is used in which a transport

equation is solved for the sub-grid scale (SGS) kinetic energy [12]. The finite volume discrete ordinates model (FVDOM) is employed to solve the radiative heat transfer equation (RTE). The weighted sum of the grey gas model is used to evaluate the absorption, emission coefficients. For comparison, the Reynolds-averaged Navier-Stokes (RANS) approach has also been used with the RNG k-epsilon model for turbulence.

A finite volume (FV) method is utilized to discretize the filtered partial governing equations into a set of resolvable linear equations. For discretization, it is required to obtain fluxes of various flow variables at cell faces using the values at cell centers. The second-order Total Variation Diminishing (TVD) scheme and the Crank–Nicholson scheme are applied. The Courant–Friedrichs–Lewy (CFL) number is less than 0.5, corresponding to a physical time step at the order of $1 \times 10{-}7$ s.

### 3.3.1 Boundary and initial conditions

The diameter of the cylinder computation domain is set as 1 m and the height is 2 m based on pre-calculations of the hydrogen jet. The influence of boundaries on the evolution of the jet is checked so that no significant velocities were formed at the boundaries. The side, top, and bottom boundaries of the domain are set as open atmosphere, in which the boundary does not influence the flow across the domain. The hydrogen inlet is circular and is located at the center of the bottom plane. Due to the high reservoir pressure of hydrogen, the throat of the nozzle can remain at higher than ambient pressure and, consequently, form an under-expanded jet from the nozzle. For the nozzle conditions the model described in Section 3.1.1 was used [6] and the notional nozzle model which is based on mass and energy conservation equations [13] but with NIST EoS was employed. Hydrogen was injected from the bottom of the computational domain with a constant upward velocity. The direction of gravity is perpendicular to the direction of the hydrogen jet to model a horizontal jet. Initially, the domain was set to be filled with stagnant air at Ta = 293 K and the ambient pressure is Pa = 1 atm. The mesh resolution was 2 mm near the national nozzle and it increase gradually further away with total of 20 million cells. This means that the eddy with the size above 2 mm is resolved in the critical region of jet initiation and the turbulence at the scales below 2 mm is assumed to be isotropic and homogeneous.

## 4.0 RESULTS AND DISCUSSION

As mentioned in Section 2.0 the concentration time series cannot be considered reliable due to the sensors experimental configuration that lead to significant time delay. Measurements of temperature in the exact position as H2-sensors could derive concentration time series by applying the adiabatic mixing approach. In this way they could provide useful information regarding the arrival time of peak concentrations and the concentration gradients. This practice can be followed by experimentalists in the future for similar applications and sensors' setup.

The comparison between predictions and experiment will be performed using the temperature time series and the decay rate of the minimum temperature along the jet centerline. However, the experimental and predicted concentration time series are also presented in Figure 5 as they can support the discussion. In the experimental time series no time synchronization has been applied (except for the response time of the valve, see Section 2.0). The UWAR simulations have currently reached only 1.2 sec physical time due to the computational cost for transient LES. The smaller figure within Figure 5 is a close view of the results until 1.2 sec (for better evaluation of UWAR simulations).

Based on the concentration time series the simulations give similar results. The experimental time delay of the mixture arrival at all sensor locations is shown. The largest delay observed is around 7 sec at the furthest sensor, C3. On the contrary, in the simulations the peak concentration is achieved at almost time zero. Differences between predictions and experiment can be also found in concentration gradient and peak concentration. Simulations exhibit steeper gradient at the early stage of the blowdown at all sensors and predict higher peak concentration. Nonetheless, as mentioned above this comparison cannot be considered reliable. At later stage and until 4 sec when release velocity is lower, the simulations gradients are in better agreement with experiment further supporting the assumption that time delay in H2-sensors is dependent on the flow conditions.

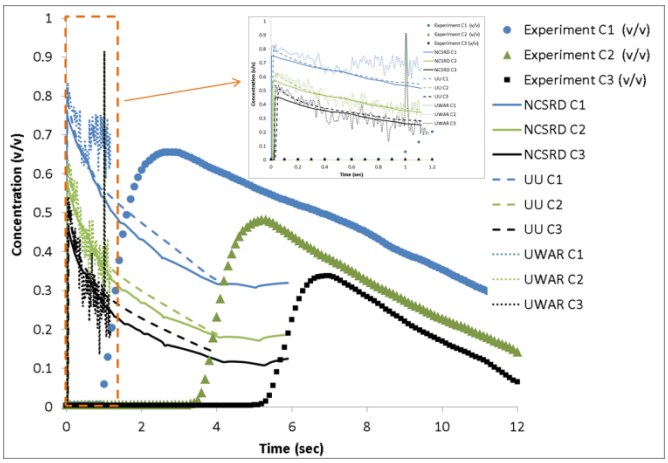


Figure 5. Concentration time series. The smaller figure is a view of the results until 1.2 sec (for better evaluation of UWAR simulations).

Figure 6 (top) shows the temperature time series at all monitoring points, while Figure 6 (bottom) shows the temperate decay rate along the jet centerline taking into account the minimum values. Based on the temperature time series along release centreline (Figure 6, top, left) very good agreement is found between experiment and simulations for the centerline sensors except for UWAR predictions close to the nozzle which exhibits serious under-prediction. The minimum temperature is predicted earlier than experiment in all simulations. This can be attributed to the time that is required for the valve to fully open. This time delay was not taken into consideration in experimental time synchronization.

Based on the temperature time series for the sensors not aligned with the release centerline (Figure 6, top, right) all simulations under-estimated the temperature at the distance closest to the nozzle, sensor T8. At the furthest sensor, T9, UU is in good agreement with the experiment, whilst NCSRD overestimates the temperature. This overestimation is higher at the initial stage of the blowdown and is reduced as release progresses. LES simulation (UWAR) over-predicts the temperature after 0.4 s. In all temperature sensors the gradient of temperature with respect to time is well reproduced by both RANS simulations for the first 4 sec of blowdown. LES simulation tends to predict a steeper temperature gradient. As far as the minimum temperature is concerned (Figure 6, bottom) all simulations tend to underestimate it, with RANS simulations to be in fairly good agreement with the experiment.

The under-prediction of temperature close to the nozzle implies that the nozzle or the notional nozzle temperature might be lower than in reality. The shock waves in the under-expanded region could warm up the mixture, a heat input that is not taken into account in the notional approaches, leading to higher temperatures. This phenomenon should be further investigated. A fully CFD simulation in the under-expanded region could provide an insight.

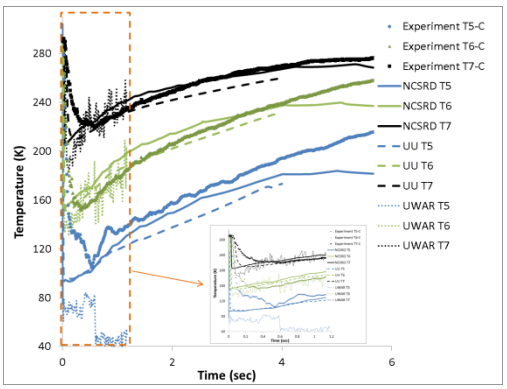


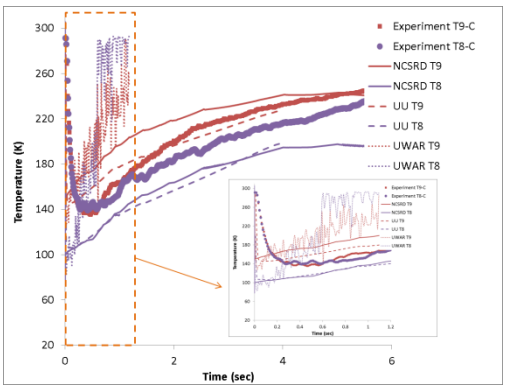

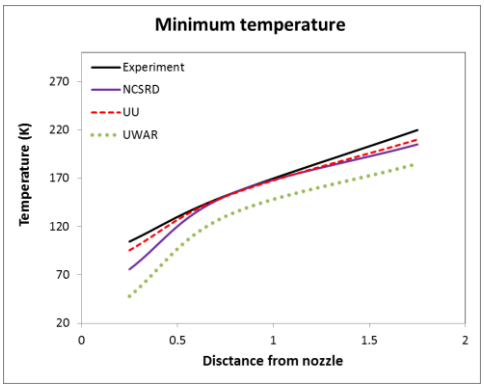


Figure 6. Temperature time series (top) at all sensors and minimum temperature decay rate (bottom) along jet centreline. The smaller figure (inside Figure, left) is a view of the results until 1.2 sec (for better evaluation of UWAR simulations).

In general, the small differences between the RANS predictions can be attributed to the different release conditions. The notional approach that UU uses assumes sonic velocity and temperature lower than the nozzle temperature based on the enthalpy conservation, while NCSRD imposes supersonic velocity and higher temperatures (equal to nozzle temperature). The different turbulent $Pr_t$ number between simulations could also lead to different level of mixing and discrepancies between predictions.

The predicted concentration and temperature contour plots on xz release plane at 0.5 and 2 sec are shown in Figure 7 for NCSRD and UU simulations. Based on both simulations the jet is momentum dominant and no buoyancy of the flammable mixture is observed.

| | Temperature (K) | Concentration (v/v) |
|---|---|---|
| NCSRD | 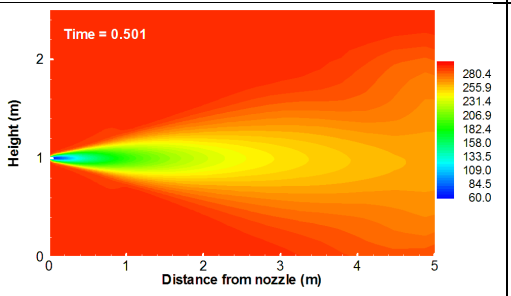 | 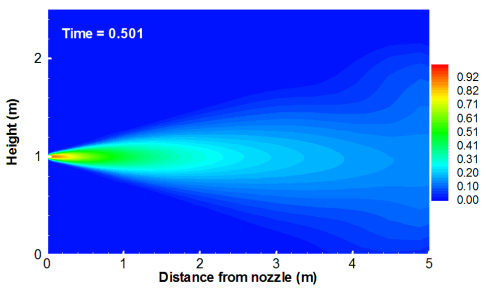 |
| UU | 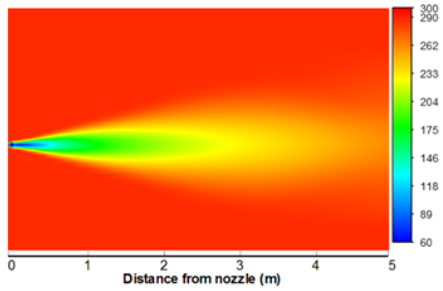 | 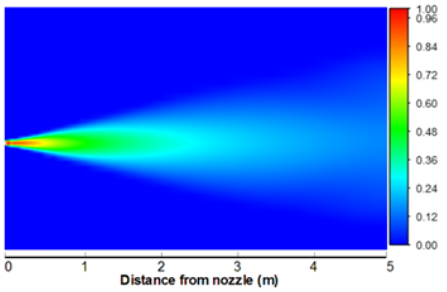 |

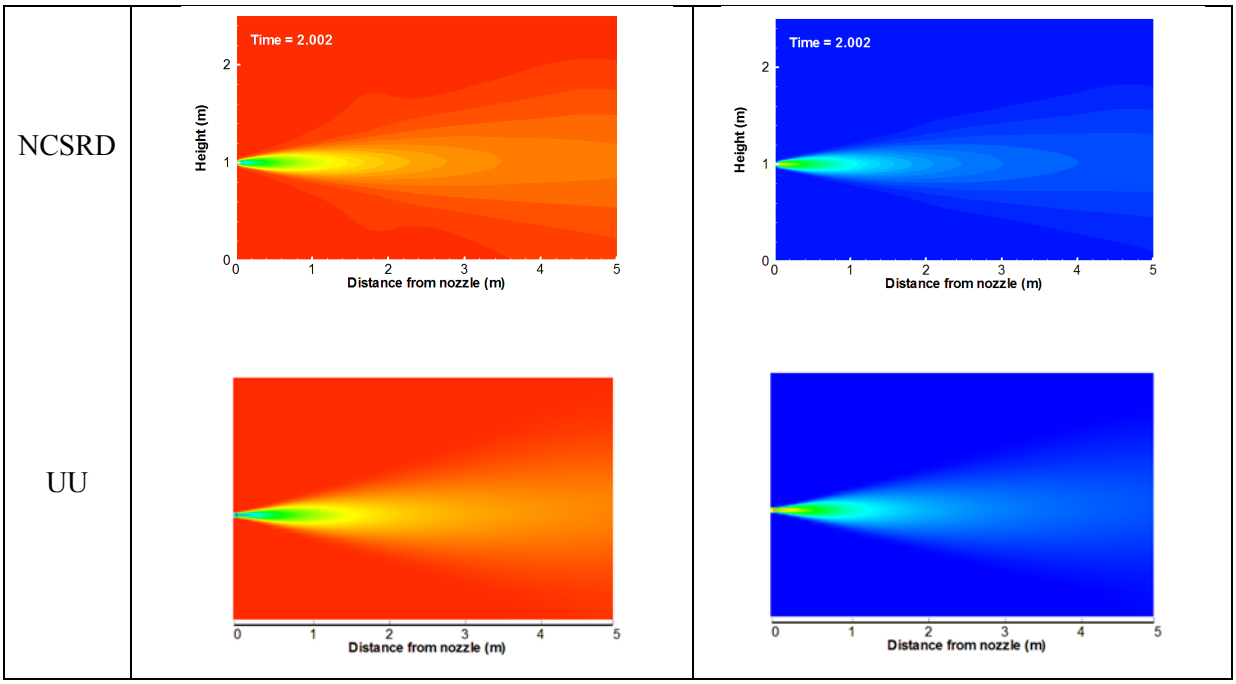


Figure 7. Temperature (left) and concentration (right) contour plots on xz release plane at two times. The contour levels of the partners are similar, but not exactly the same due to software constrains in post-processing.

Finally, UWAR performed a comparison between LES and RANS simulations using the same numerical parameters (Figure 8). Currently the results up to 1.2 sec are available. It is found that the LES predicts a more rapid dispersion of hydrogen than RANS. The temperature and hydrogen mole fraction predicted by LES have a more rapid decrease (and increase, respectively) at the early stage of the blowdown, especially for the downstream sensors of T7 and C3. The instantaneous distributions of hydrogen mole fraction and temperature during the initial stage of the jet are presented in Figure 9.

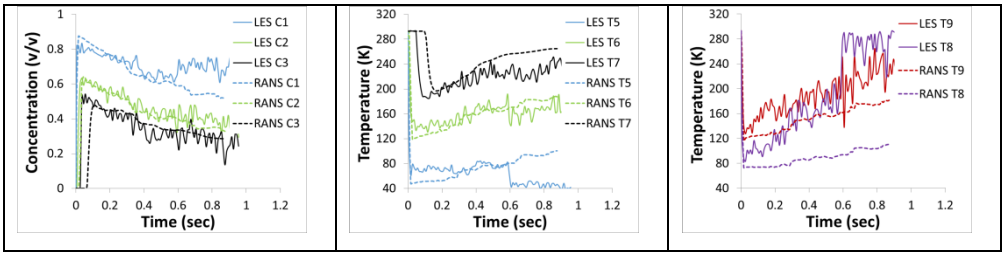


Figure 8. Comparison of the results between LES and RANS: hydrogen concentration of sensors C1, C2 and C3 (left), (b) temperature of sensors T5, T6 and T7 (center), (c) temperature of sensors T8 and T9 (right).

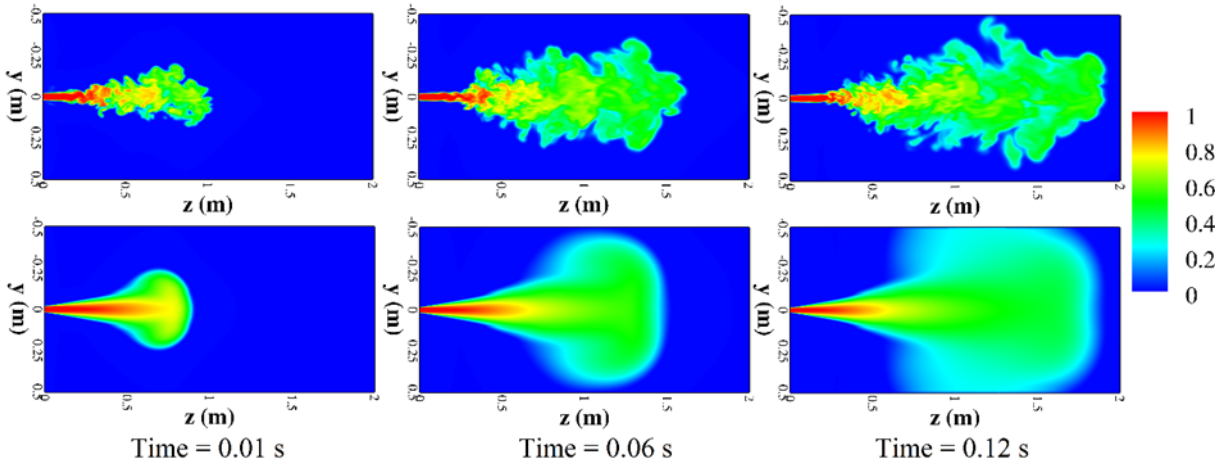

Figure 9. Instantaneous distributions of hydrogen mole fraction from 0.01 s to 0.12 s: LES results (top) and RANS results (bottom).

## 5.0 CONCLUSIONS

Simulations of hydrogen dispersion resulting from high-pressure cryogenic blowdown release were performed within the EU-funded PRESLHY project and the results are presented here. Three partners, NCSRD, UU, and UWAR simulated the experiments. The partners used different methodologies to calculate the blowdown conditions: NCSRD and UWAR uses the experimental transient tank conditions and performs isentropic expansion taking into account the discharge line losses for every measured time. UU uses a non-adiabatic model starting from initial tank conditions. The non-adiabatic model with a discharge coefficient of 0.7 calculated lower mass flow rate than measurements at the initial stage of the release. To model the under-expanded jet different notional nozzle approaches were employed. The approach that NCSRD used calculated higher velocity and temperature than the approach that UU and UWAR used.

Comparison between predictions and experiment showed a fairly good agreement in terms of temperature during the entire blowdown. However, LES simulation significantly underestimated the temperature close to the nozzle. The decay rate of minimum temperature along the jet centerline is under predicted close to the nozzle, while is predicted with higher accuracy further downstream the nozzle. This indicates that either the calculated nozzle temperature or the notional nozzle temperature computed by both methodologies/approaches is lower than the experiment. Comparison between UWAR-LES and UWAR-RANS simulations with the same numerical setup showed that LES predicts a more rapid dispersion at distances close to the nozzle.

Comparison between predicted concentrations and measurements showed significant discrepancies in the arrival time. The predicted arrival time occurred at almost time zero in all sensors, while in experiment there was a different time delay in each sensor with the largest delay to be around 7 sec for the sensor furthest away from the nozzle.

The experimentally observed delay in hydrogen concentration arrival time is attributed to the sensors' experimental setup. Hydrogen-air mixture was sucked from the nominal sensor experimental location via a long thin plastic tube, using a small pump, before reaching the hydrogen sensor itself. Although the experimentalists accounted for a time delay generated by this arrangement, and corrected homogeneously all the measured concentration time histories, this delay was estimated at separate tests (using hydrogen balloons) with widely different conditions and seems a) to be underestimated and b) different for each sensor location, i.e. depending on the flow conditions.

Through this work the need for further future research is revealed for measuring concentration close to the source for under-expanded hydrogen jets. Due to the difficulties encountered it is recommended for future experiments near the source to a) reduce the length of the plastic tube as much as possible and b) use collocated temperature sensors at nominal sensor locations. Collocated temperature sensors can be used to derive hydrogen concentration, using the adiabatic mixing approach and in this sense can be used to check the reliability of hydrogen concentration readings. An alternative option to reduce the time delay could be to use a more powerful pump for suction. Such an option though was not possible in the present experiments as it would lead to flow velocities hitting the hydrogen sensor out of the sensor's specifications.

## 6.0 ACKNOWLEDGMENTS

The research leading to these results was financially supported by the PRESLHY project, which has received funding from the Fuel Cells and Hydrogen 2 Joint Undertaking under grant agreement No 779613. This Joint Undertaking receives support from the European Union's Horizon 2020 research and innovation programme, Hydrogen Europe and Hydrogen Europe research.

## REFERENCES

[1] A. Veser, A. Friedrich, M. Kuznetsov, T. Jordan, and N. Kotchourko, "Hydrogen blowdown release experiments at different temperatures in the DISCHA-facility," in *International*

*Conference on Hydrogen Safety, Edinburgh, UK, September 21-23*, 2021, paper submitted.

[2] A. D. Birch, D. R. Brown, M. G. Dodson, and F. Swaffield, "The Structure and Concentration Decay of High Pressure Jets of Natural Gas," *Combust. Sci. Technol.*, vol. 36, no. 5–6, pp. 249–261, Apr. 1984.

[3] E. Papanikolaou and D. Baraldi, "Evaluation of notional nozzle approaches for CFD simulations of free-shear under-expanded hydrogen jets," *Int. J. Hydrogen Energy*, vol. 37, pp. 18563–18574, 2012.

[4] X. Li, D. M. Christopher, E. S. Hecht, and I. W. Ekoto, "Comparison of two-layer model for hydrogen and helium jets with notional nozzle model predictions and experimental data for pressures up to 35 MPa," *Int. J. Hydrogen Energy*, vol. 42, no. 11, pp. 7457–7466, 2017.

[5] A. G. Venetsanos, E. Papanikolaou, and J. G. Bartzis, "The ADREA-HF CFD code for consequence assessment of hydrogen applications," *Int. J. Hydrogen Energy*, vol. 35, no. 8, pp. 3908–3918, Apr. 2010.

[6] A. G. Venetsanos, S. G. Giannissi, I. C. Tolias, A. Friedrich, and M. Kuznetsov, "Cryogenic and ambient gaseous hydrogen blowdown with discharge line effects," in *International Conference on Hydrogen Safety, Edinburgh, UK, September 21-23*, 2021, paper submitted.

[7] A. G. Venetsanos and S. G. Giannissi, "Release and dispersion modeling of cryogenic under-expanded hydrogen jets," *Int. J. Hydrogen Energy*, vol. 42, no. 11, pp. 7672–7682, 2016.

[8] D. Molkov, V., Dadashzadeh, M., Kashkarov, S., and Makarov, "Performance of hydrogen storage tank with TPRD in an engulfing fire," *Int. J. Hydrog. Energy*, vol. submitted, 2021.

[9] V. Bell, Ian H. and Wronski, Jorrit and Quoilin, Sylvain and Lemort, "Pure and Pseudo-pure Fluid Thermophysical Property Evaluation and the Open-Source Thermophysical Property Library CoolProp," *Ind. \& Eng. Chem. Res.*, vol. 53, no. 6, p. 2498—2508, 2014.

[10] V. Molkov, D. Makarov, and M. Bragin, "Physics and modelling of underexpanded jets and hydrogen dispersion in atmosphere," in *Physics of extreme state of matter 2009 (selected papers presented at the XXIII International Conference on Interaction of Intense Energy Fluxes with Matter, Elbrus,1-6 March 2009)*, 2009, pp. 146–149.

[11] V. Cirrone, D., Makarov, D. and Molkov, "Cryogenic hydrogen jets: flammable envelope size and hazard distances for jet fire," in *International Conference on Hydrogen Safety, Adelaide, Australia*, 2019, pp. 1–9.

[12] A. Yoshizawa, "Bridging between eddy-viscosity-type and second-order turbulence models through a two-scale turbulence theory," *Phys. Rev. E*, vol. 48, no. 1, p. 273, 1993.

[13] V. Molkov and M. Bragin, "High-pressure hydrogen leak through a narrow channel," *Nonequilibrium Phenom. Plasma, Combust. Atmos.*, pp. 332–338, 2009.